ISSN 2616-5880 Vol. 6, Issue 3: 19-29, DOI: 10.25236/AJMC.2025.060302

Enhancing Tetracycline Degradation through Nitrogen-Deficient G-C_3N_4/BiOCl Heterojunction with Upconversion Photocatalysis

Weiyang Chen[1,a,*], Jingjing Xu[1,b]

[1]*School of Environmental Science and Engineering, Nanjing University of Information Science & Technology, Nanjing, China*
[a]*cwy873238455@163.com*, [b]*Xujj@nuist.edu.cn*
**Corresponding author*

Abstract: *The heterojunction photocatalyst nitrogen-deficient g-C_3N_4/BiOCl (CNBOC) was synthesized via in-situ calcination coupled with hydrothermal methods. Under visible-light irradiation (λ > 510 nm), the CNBOC-2 composite demonstrated enhanced photocatalytic activity for tetracycline hydrochloride (TC) degradation, achieving 86.2% removal within 60 min. The composite also exhibited excellent cycling stability, retaining ~70% degradation efficiency after four successive cycles. Photoluminescence (PL) characterization revealed that the nitrogen-deficient g-C_3N_4 upconversion agent effectively absorbed near-infrared light (~850 nm) and emitted yellow-green light (~570 nm).*

Keywords: *Photocatalytic, Upconversion, Tetracycline, C_3N_4*

1. Introduction

Tetracycline antibiotics (TCs), as one of the most common emerging contaminants in water pollution, have drawn significant attention due to their environmental behavior and ecological risks. Produced by actinomycetes, these broad-spectrum antibacterial agents pose major challenges in global water management because of their chemical stability and residue accumulation from extensive use. TCs can cause permanent tooth discoloration, enamel hypoplasia in humans, and fetal skeletal growth inhibition [1]. They react with various acids and bases to form salts, with tetracycline hydrochloride (TC)being the most representative. Due to its low cost and excellent stability, TC has become the second most used antibiotic worldwide, widely applied in livestock and aquaculture industries [2]. However, TC's poor biodegradability leads to environmental accumulation, creating selective pressure on aquatic bacteria that may promote antibiotic-resistant strains, thereby threatening human and animal health [3].

Graphitic carbon nitride (g-C_3N_4), composed of Earth-abundant elements, is a widely studied semiconductor photocatalyst with stable chemical properties. It exhibits visible-light absorption, suitable band structure, and predictable light response [4]. Researchers have extensively applied it in hydrogen production and photocatalytic studies. Duan et al. [5] developed an exfoliation-ultrasonication method to prepare carbon nitride quantum dots/nanosheet composites for simultaneous hydrogen generation and dye degradation under visible light. Liu et al. [6] fabricated layered double hydroxide/g-C_3N_4 composite membranes demonstrating effective photocatalytic dye removal and self-cleaning capabilities in flowing wastewater. g-C_3N_4 also shows potential in upconversion applications. Huang et al. [7] reported graphene oxide aerogels modified with g-C_3N_4 quantum dots achieving UV-to-NIR light response through hydrothermal-vacuum injection methods. Chen et al. [8] utilized NaYF4:Yb^{3+}/Tm^{3+} upconversion nanoparticles with g-C_3N_4 quantum dots to convert infrared to UV/visible light, enabling innovative photodynamic therapy applications in bioimaging.

This chapter presents an N-deficient g-C_3N_4/BiOCl heterojunction upconversion photocatalyst for degrading 5 ppm TC wastewater under λ>510 nm light. The system demonstrated high photocatalytic activity and stability, with comprehensive characterization (including PL analysis) revealing its degradation mechanism.

ISSN 2616-5880 Vol. 6, Issue 3: 19-29, DOI: 10.25236/AJMC.2025.060302

2. Experimental section

2.1 Synthesis of C_3N_4; BiOCL and CNBOC

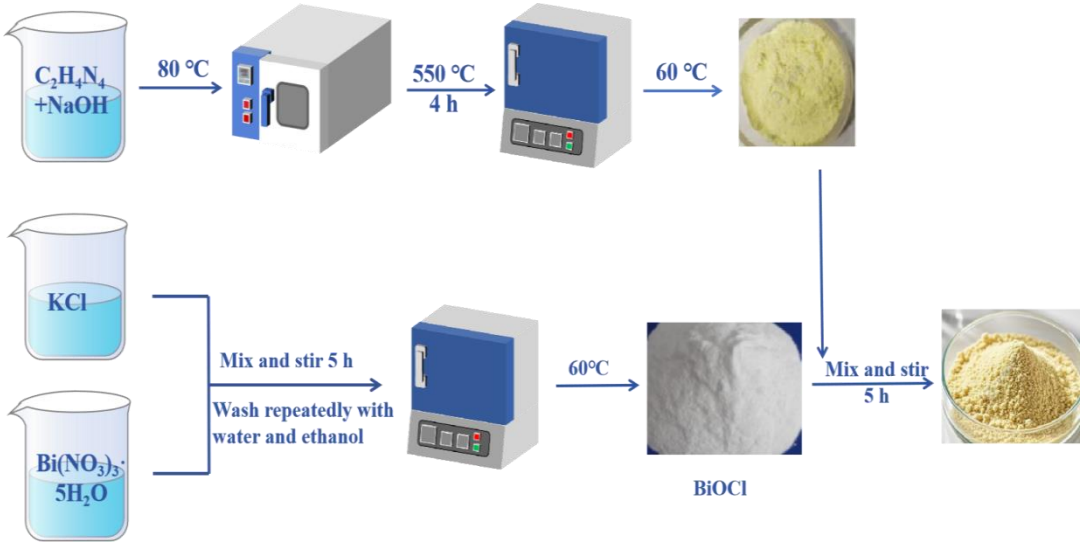

Figure 1 Schematic illustration of CNBOC composite synthesis

BiOCl was synthesized via a coprecipitation method [9]. Specifically, 5 mmol $Bi(NO_3)_3$ $5H_2O$ was dissolved in 50 mL deionized water under 30-minute stirring. Subsequently, 5 mmol KCl was added to form a milky suspension after 5 h continuous agitation. The product was centrifuged, washed repeatedly with deionized water and ethanol, then dried at 60 ℃ to obtain white BiOCl powder (denoted as BOC).

Nitrogen-deficient g-C_3N_4 nanosheets were prepared through in-situ calcination [10]. Initially, 1.11 g NaOH was dissolved in 30 mL deionized water, followed by dispersing 10 g dicyandiamide into the solution. After 10-minute stirring, the homogeneous suspension was dried at 80 ℃. The resultant white crystals were calcined in a muffle furnace (heating rate: 10 °C min^{-1} to 550 °C, maintained for 4 h). The cooled product was washed and dried at 60 ℃, yielding pale yellow modified CN powder.

The g-C_3N_4/BiOCl composites were synthesized by electrostatic self-assembly. Specifically, 0.2 g CN was mixed with 0.15 g, 0.3 g, or 0.5 g BOC in 30 mL deionized water under 6 h stirring. After washing and drying at 60 ℃, three composite samples (CNBOC-1, CNBOC-2, CNBOC-3) were obtained as white powders. The preparation process is illustrated in Figure 1.

2.2 Photocatalytic Activity Evaluation

The photocatalytic reactions were conducted under a 300 W xenon lamp with wavelength cutoff (λ >510 nm). The target pollutant was 5 ppm tetracycline (TC) solution. During illumination, 4 mL aliquots were collected every 15 min (total reaction time: 60 min). After centrifugation, the supernatant's absorbance was measured by UV-vis spectrophotometer to calculate the degradation efficiency.

3. Results and Discussion

3.1 Structural Characteristics

The phase purity and crystalline structure of synthesized samples were characterized by X-ray diffraction (XRD) under test conditions: 2θ range 10°-80 °, scan rate 7 °min^{-1}. As shown in Figure 2, the BOC sample exhibited characteristic peaks corresponding to (101), (110), and (102) crystal planes (JCPDS No.06-0249), indicating high crystallinity. The composite samples showed additional weak peaks at the (002) plane of CN, likely due to its low content. Figure 2a confirms the coexistence of both BOC and CN phases without impurity peaks, demonstrating successful composite preparation with well-defined crystallinity.

ISSN 2616-5880 Vol. 6, Issue 3: 19-29, DOI: 10.25236/AJMC.2025.060302

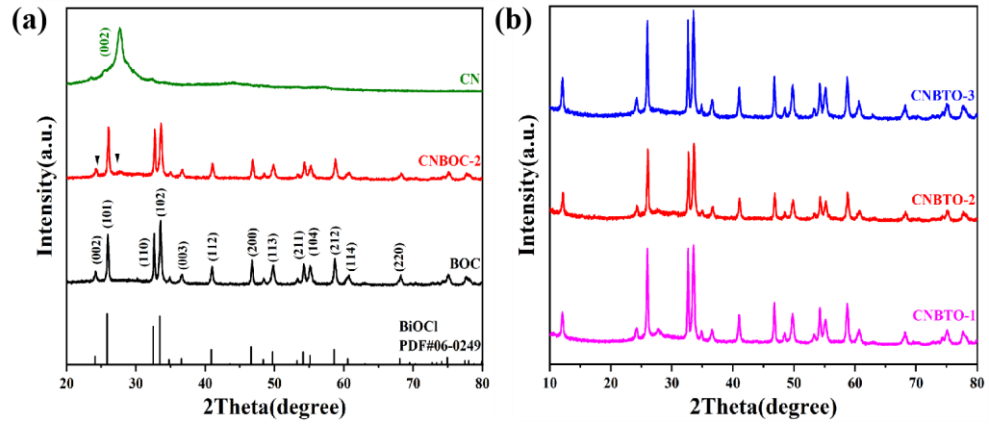

Figure 2 XRD patterns of CN, BOC, and CNBOC composites

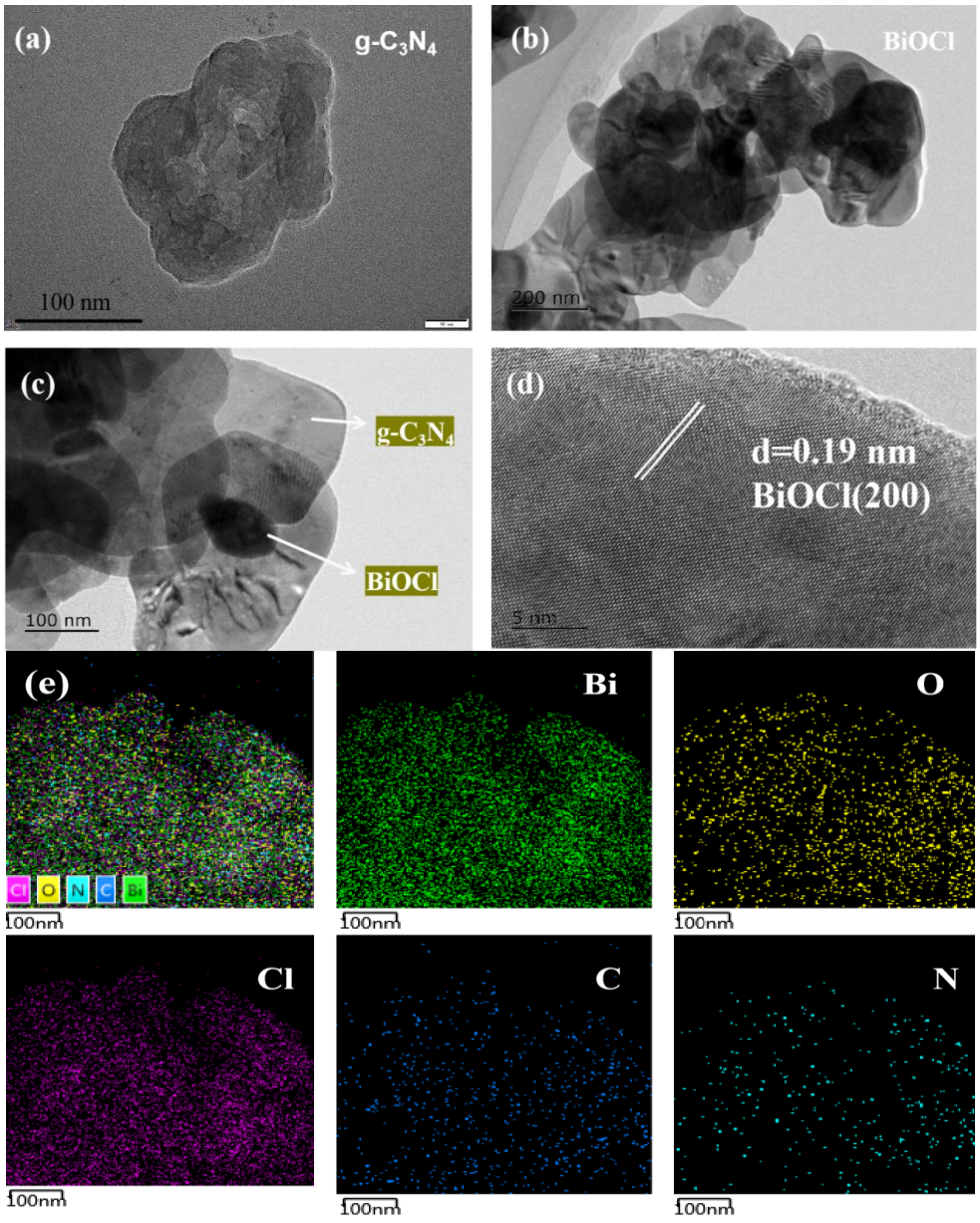

Figure 3 (a) TEM image of CN; (b) TEM image of BOC; (c,d) HRTEM images of CNBOC-2; (e) EDS elemental mapping of CNBOC-2

The surface morphology and microstructure of CN, BOC, and CNBOC-2 samples were investigated

ISSN 2616-5880 Vol. 6, Issue 3: 19-29, DOI: 10.25236/AJMC.2025.060302

by TEM and HRTEM. Figure 3a shows pure CN exhibiting stacked multilayer nanosheets. In Figure 3b, pure BOC displays smooth-surfaced nanosheets with ultrathin thickness and well-defined edges, both showing lamellar nanostructures. TEM characterization in Figure 3c confirms BOC nanosheets uniformly distributed on the CN substrate while maintaining their original layered structures. Stable hetero-contact formed through interfacial coupling between CN and BOC plays a vital role in photocatalysis. This interfacial configuration effectively promotes charge carrier separation/transfer and enhances photocatalytic activity. Moreover, the tight interface increases active site exposure and strengthens reactant adsorption/activation on the catalyst surface, further improving photocatalytic performance [11].

The HRTEM image in Figure 3d reveals lattice fringes corresponding to BOC crystallites, with 0.19 nm spacing matching the (200) crystal plane of BOC. Elemental distribution on the CNBOC-2 composite surface was analyzed by Energy Dispersive X-ray Spectroscopy (EDS), as shown in Figure 3e. C, N, Bi, O, and Cl elements exhibit uniform distribution across the composite, confirming homogeneous dispersion of BiOCl nanosheets within the g-C_3N_4 matrix and tight interfacial contact. This elemental uniformity demonstrates successful composite preparation and excellent compatibility between g-C_3N_4 and BiOCl. The TEM, HRTEM, and EDS results collectively verify the successful fabrication of CNBOC-2 composites.

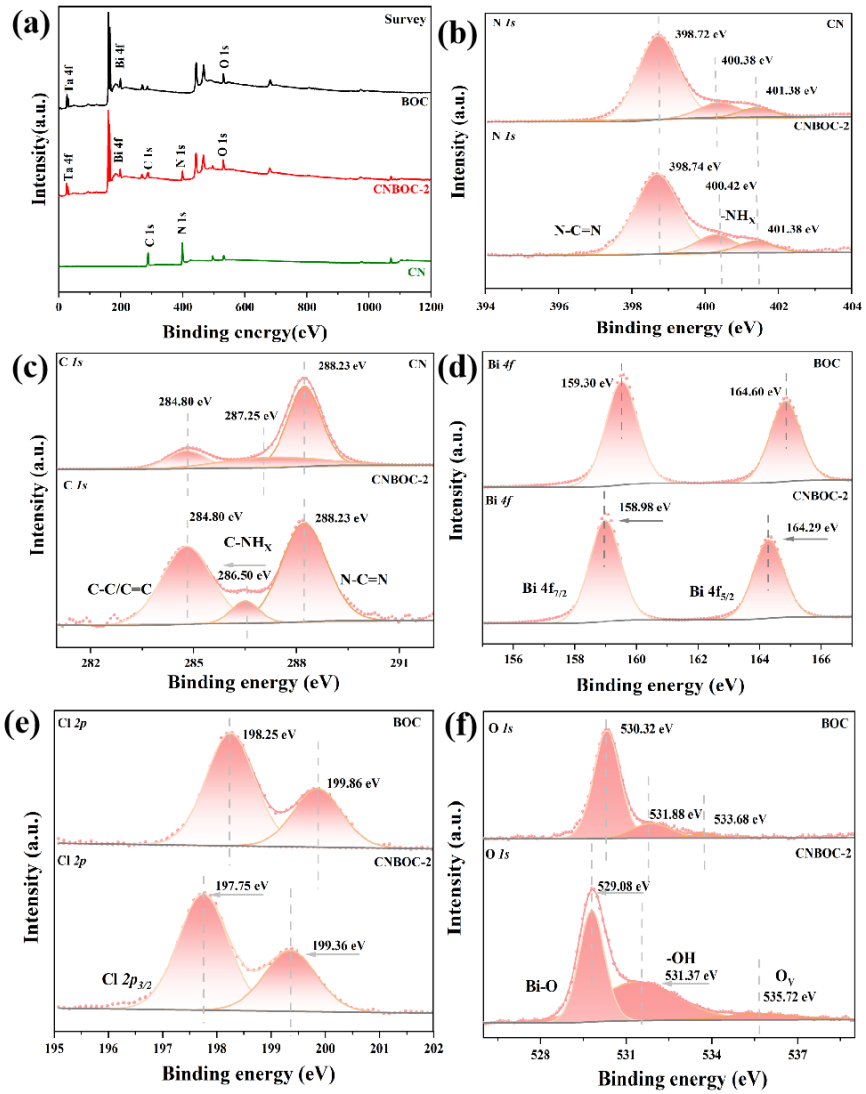

Figure 4 (a) XPS survey spectra; (b) High-resolution N 1s spectra; (c) High-resolution C 1s spectra; (d) High-resolution Bi 4f spectra; (e) High-resolution Cl 2p spectra; (f) High-resolution O 1s spectra

The surface chemical states and interfacial bonding characteristics of the CN/BOC heterojunction system were systematically characterized by X-ray photoelectron spectroscopy (XPS) depth profiling. High-resolution XPS spectra of N 1s, C 1s, Bi 4f, Cl 2p, and O 1s are displayed in Figures 4a-f. For

ISSN 2616-5880 Vol. 6, Issue 3: 19-29, DOI: 10.25236/AJMC.2025.060302

pure CN, characteristic peaks at 398.72 eV, 400.38 eV, and 401.38 eV correspond to N 1s orbitals [12], while peaks at 284.80 eV, 287.25 eV, and 288.23 eV originate from C 1s orbitals, consistent with reported values [13].

In pure BOC, the peak at 159.3 eV is assigned to Bi $4f_{7/2}$, and the peak at 164.60 eV corresponds to Bi $4f_{5/2}$ (Figure 4f), confirming the Bi^{3+} state. Peaks at 198.25 eV and 199.86 eV arise from Cl 2p orbitals. O 1s orbital contributions are observed at 530.32 eV, 531.88 eV, and 533.68 eV, with the 533.68 eV binding energy attributed to surface-adsorbed OH or H_2O groups [14].

For CNBOC-2 composite, three O 1s peaks at 529.08 eV, 531.37 eV, and 535.72 eV correspond to lattice -OH and oxygen vacancies (OV). XPS analysis reveals binding energy shifts in CNBOC-2: C 1s,Bi 4f, and Cl 2p orbitals show negative shifts compared to individual components, whereas N 1s and O 1s orbitals exhibit positive shifts. These shifts indicate electron transfer behavior between constituents - Bi/Cl atoms in BOC act as electron donors transferring electrons to N sites in the CN framework. These results confirm molecular-level integration of CNBOC composites and successful heterojunction formation.

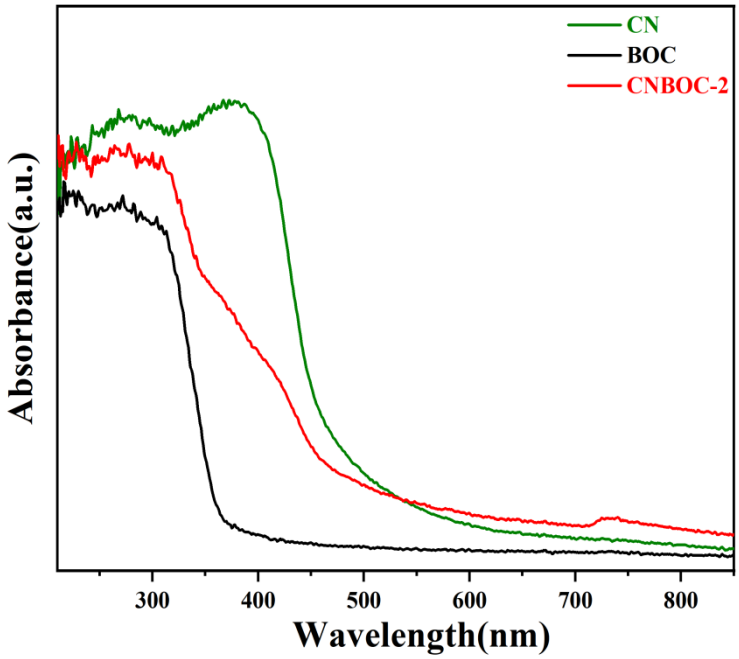

Figure 5 DRS spectra

The light response characteristics of the materials were systematically characterized using diffuse reflectance spectroscopy (DRS). Figure 5 shows pure BTO exhibiting light absorption primarily in the 200-410 nm range with limited intensity, showing an absorption edge near 410 nm. Pure CN demonstrates broadband light response across 200-850 nm, indicating effective absorption of ultraviolet, visible, and near-infrared light.

The CNBOC-2 composite exhibits a red-shifted absorption edge compared to pure BOC, maintaining light absorption capability in the 510-850 nm range. This suggests that the composite inherits CN's broad-spectrum absorption properties while combining with BOC, enabling extended wavelength photon harvesting.

The Kubelka-Munk theory model was employed to calculate the band gap (Eg) of CN and BOC, providing insights into their light absorption edge characteristics [15]:

$$\alpha h\nu = A(h\nu - Eg)$$

The parameters in this equation are defined as follows: α (absorption coefficient), h (Planck's constant), ν (incident light frequency), and A (material-dependent constant). The transition index n is determined by semiconductor band transition type - n=1 for direct bandgap material CN and n=4 for indirect bandgap material BOC [16]. Band gap calculations yield Eg values of 2.7 eV for CN and 3.25 eV for BOC (Figures 6a-b), consistent with literature [17].

The band structures were analyzed to understand photocatalytic mechanisms. Mott-Schottky (M-S)

ISSN 2616-5880 Vol. 6, Issue 3: 19-29, DOI: 10.25236/AJMC.2025.060302

plots reveal semiconductor types: Both pure BOC and CN show positive slopes in Figures 6c-d, confirming n-type characteristics [18]. In n-type semiconductors, the Fermi level (E_F) approaches the conduction band edge (E_{CB}), causing a ~0.1 eV positive shift in valence band edge (E_{VB}) relative to flat-band potential (E_{fb}) [19]. Experimental E_{fb} measurements give -0.51 V (BOC) and -0.76 V (CN) vs. NHE, corresponding to E_{CB} values of -0.51 eV and -0.76 eV, respectively.

Using the relationship $E_{VB} = E_{CB} + Eg$, calculated E_{VB} values are 2.84 eV (BOC) and 2.04 eV (CN), matching reported data [20].

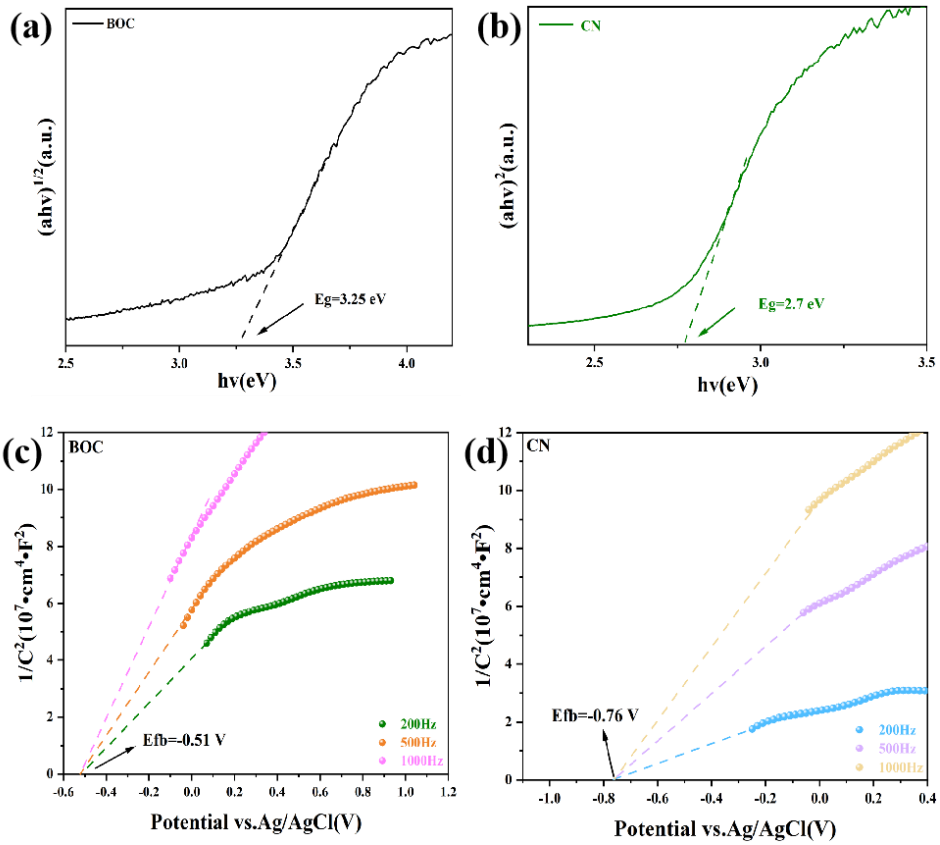

Figure 6 (a) (αhv)1/2 vs. hv plots for BOC; (b) (αhv)2 vs. hv plots for CN; (c,d) Mott-Schottky (MS) plots for BOC and CN, respectively

3.2 Photocatalytic Performance Analysis

The photocatalytic activity of synthesized samples was evaluated through tetracycline (TC) degradation under visible-light irradiation ($\lambda > 510$ nm). As shown in Figure 7a, pure CN and BOC exhibit poor degradation performance, achieving only 14.6% and 25.7% TC removal within 60 min, respectively. The CN/BOC heterojunction system demonstrates significantly enhanced photocatalytic activity compared to individual components, attributed to improved interfacial charge transfer and suppressed carrier recombination.

After 60-min illumination, CNBOC-1 and CNBOC-3 show TC degradation efficiencies of 73.4% and 72.1%, respectively. Notably, CNBOC-2 achieves the highest degradation efficiency of 86.2% under identical conditions, confirming its optimal mass ratio (CN:BOC = 2:3). The apparent kinetic constants (k) for TC degradation by different photocatalysts are presented in Figure 7b, calculated through first-order kinetic fitting [21]:

$$\ln(C_0/C_t)=kt$$

C_0 represents the initial TC concentration before illumination (mg Ł$^{-1}$), and C_t denotes the TC concentration at reaction time t (min). The kinetic constant k has units of min^{-1}. Figure 7b reveals that the CNBOC-2 composite exhibits the highest apparent rate constant (0.0346 min^{-1}), demonstrating 10.17 fold and 7.68 fold enhancements compared to pure CN and BOC, respectively.

ISSN 2616-5880 Vol. 6, Issue 3: 19-29, DOI: 10.25236/AJMC.2025.060302

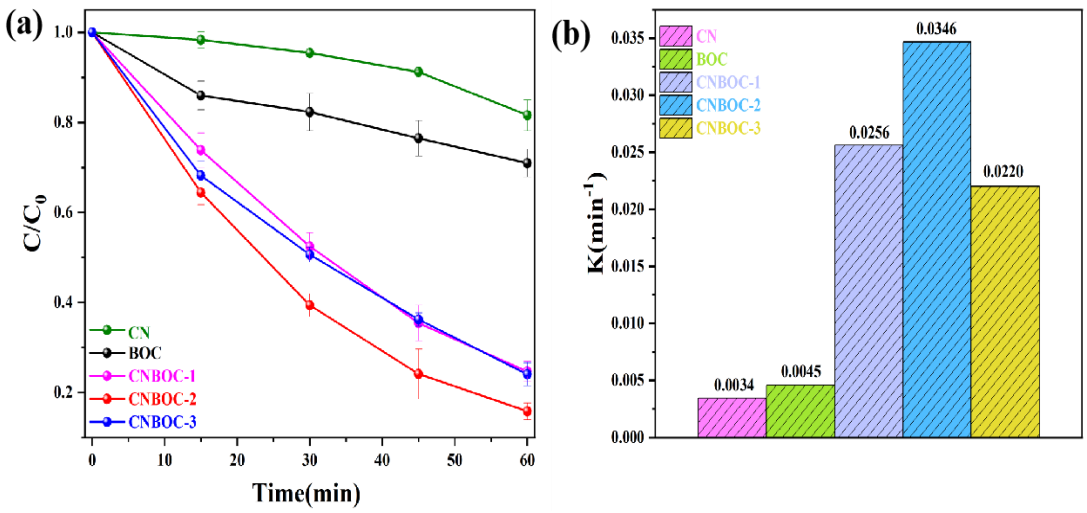

Figure 7 (a) TC degradation curves of different samples under visible-light irradiation (λ > 510 nm); (b) Apparent kinetic constants for TC degradation

The photocatalytic stability, as a crucial quality indicator alongside activity, was systematically evaluated. As shown in Figure 8a, CNBOC-2 composite maintains stable photocatalytic performance through four recycling experiments under visible-light irradiation (λ > 510 nm). The degradation efficiency retained approximately 70% in the final cycle, showing only 16.2% reduction compared with the initial test.

X-ray diffraction (XRD) analysis in Figure 8b reveals no noticeable shifts or emergence of new characteristic peaks after cycling tests, confirming excellent structural integrity of the composite during charge-discharge processes. This crystalline stability directly validates the outstanding cyclic performance durability of the material .

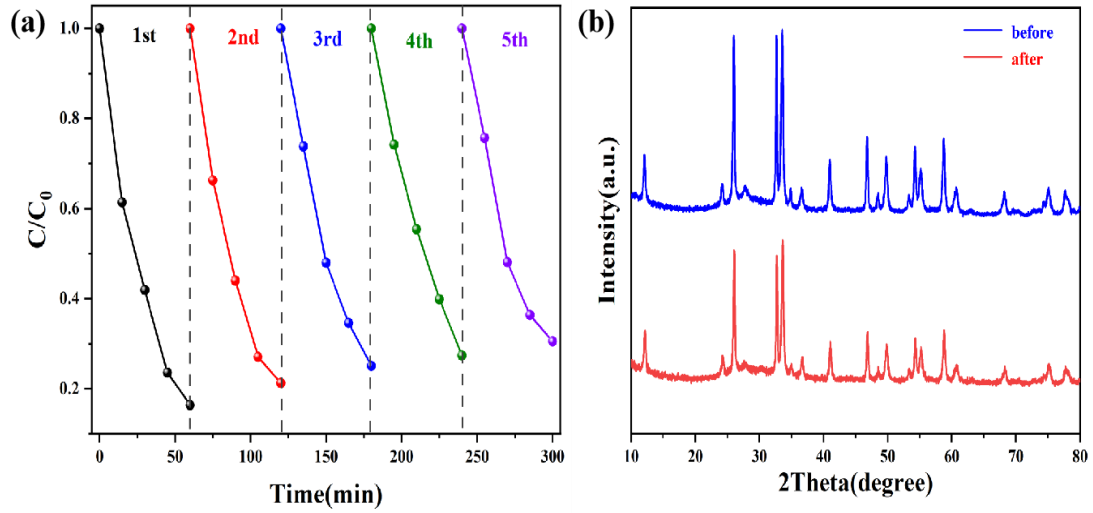

Figure 8 (a) Cycling degradation performance; (b) XRD patterns of CNBOC-2 before and after cycling tests

3.3 Photocatalytic Mechanism Analysis

The photocatalytic degradation mechanism of CN/BOC heterojunction was further investigated through photocurrent (PC), electrochemical impedance spectroscopy (EIS), and photoluminescence (PL) measurements to systematically evaluate charge carrier separation efficiency and migration dynamics. A light-dark cycling system was constructed to monitor transient photocurrent responses under intermittent illumination, revealing distinct charge transfer kinetics among catalysts.

Stronger photocurrent responses generally indicate higher carrier separation efficiency and faster interfacial charge transfer rates [22]. This phenomenon originates from effective suppression of

ISSN 2616-5880 Vol. 6, Issue 3: 19-29, DOI: 10.25236/AJMC.2025.060302

electron-hole recombination and reduced energy loss during charge migration. As shown in Figure 9b, pure CN and BOC exhibit weaker photocurrent intensities compared to composites. The CNBOC-2 composite demonstrates the strongest photocurrent response, primarily attributed to heterojunction formation that enhances charge separation, accelerates migration, and increases surface active sites.

Figure 9a presents EIS Nyquist plots for analyzing charge transfer resistance. Smaller arc radii correspond to lower charge transfer resistance and higher carrier separation efficiency [23]. The CNBOC-2 composite shows the smallest semicircle diameter, confirming superior charge separation and electrical conductivity compared to pure components and other composites.

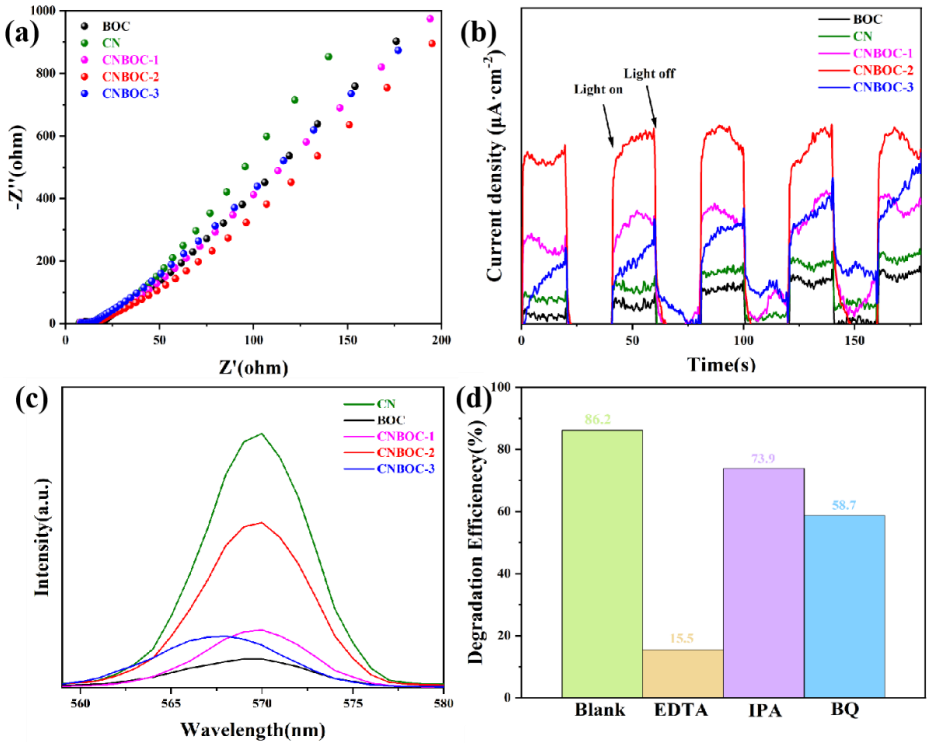

Figure 9 (a) Electrochemical impedance spectroscopy (EIS) Nyquist plots; (b) Transient photocurrent responses of different samples; (c) Photoluminescence (PL) spectra; (d) Active species trapping experiments during TC photocatalytic degradation by CNBOC-2

The upconversion properties of materials were systematically characterized by photoluminescence (PL) spectroscopy. As shown in Figure 9c, all samples exhibit characteristic emission bands in the visible region under 850 nm near-infrared excitation, with consistent peak positions confirming stable upconversion luminescence. Pure CN demonstrates the strongest emission peak at 570 nm under 850 nm excitation, revealing excellent upconversion capability of the N-deficient CN to convert near-infrared light into visible (yellow-green) emissions. In contrast, pure BOC shows negligible emission peaks under identical conditions, indicating poor upconversion performance.

Heterojunction formation significantly enhances upconversion efficiency compared to pure BOC. The CNBOC-2 composite exhibits the most pronounced upconversion performance among all composites, correlating with its superior photocatalytic activity.

Active species trapping experiments identified dominant reactive species (O_{2-} and h^+) in TC degradation by CNBOC-2. Scavengers were employed: ethylenediaminetetraacetic acid disodium (EDTA, 0.744 g) for h^+, isopropanol (IPA, 2 mL) for ·OH, and benzoquinone (BQ, 0.0003 g) for $\cdot O_{2-}$. Figure 9d shows TC degradation was significantly suppressed upon adding EDTA (h^+ scavenger) and strongly inhibited by BQ (O_{2-} scavenger), while IPA (OH scavenger) caused minimal effects. This confirms h^+ and $\cdot O_{2-}$ as primary active species driving the photocatalytic process.

Based on the experimental findings and band structure analysis, a proposed Z-scheme heterojunction mechanism for TC degradation is illustrated in Figure 10. The modified CN absorbs near-infrared light ($\lambda > 510$ nm) and emits yellow-green photons through upconversion, subsequently exciting BOC to generate electron-hole pairs.

ISSN 2616-5880 Vol. 6, Issue 3: 19-29, DOI: 10.25236/AJMC.2025.060302

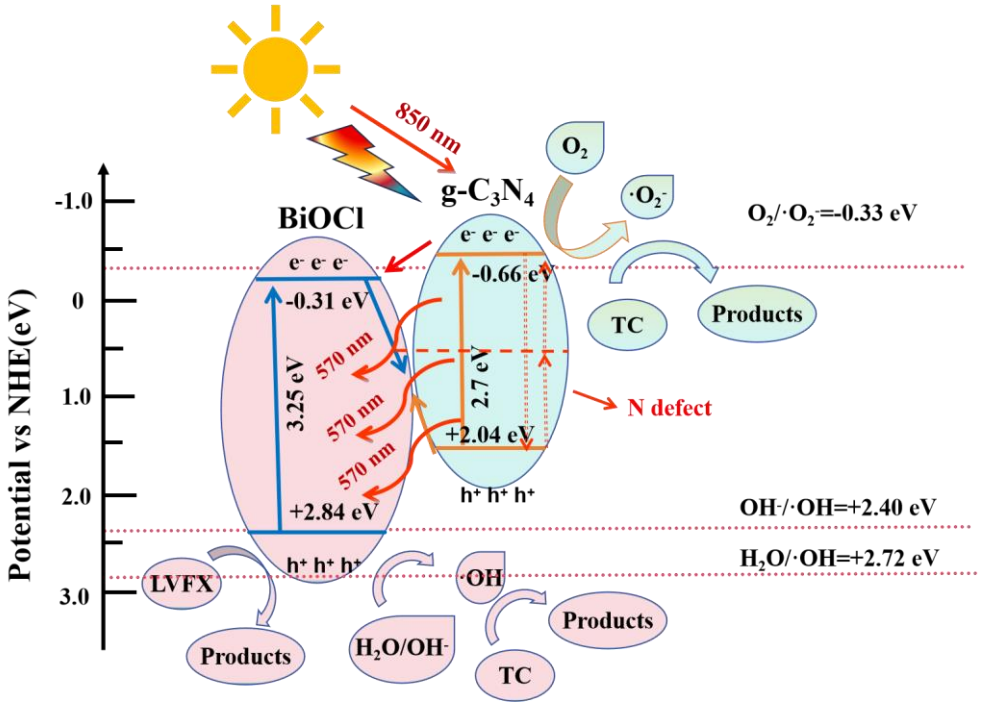

Figure 10 Proposed direct Z-scheme photocatalytic mechanism of CN/BOC composites for TC degradation

The valence band (VB) of CN (+2.04 eV) lies below the $OH^-/\cdot OH$ potential (+2.4 eV), while the conduction band (CB) of BOC (-0.31 eV) positions slightly above O_2/O_{2-} (-0.33 eV) [24]. This configuration enables O_{2-} generation but prevents OH formation, consistent with scavenging experiments.

Electrons from CN's CB transfer to BOC's CB, where accumulated electrons combine with holes from CN's VB. The strongly reductive electrons in CN's CB reduce O_2 to O_{2-}, while holes in BOC's VB (E_{VB} = +2.84 eV) exhibit sufficient oxidative potential to activate H_2O ($H_2O/$ OH: +2.72 eV).

The introduced nitrogen defect states in CN act as intermediate levels for charge carriers. Free electrons in CN sequentially absorb two low-energy photons: first transitioning to defect states, then reaching the CB. This photon emission process transfers energy to BOC, significantly enhancing charge separation/migration. Ultimately, this mechanism enables effective TC degradation under long-wavelength visible light irradiation.

4. Conclusions

A direct Z-scheme CN/BOC heterojunction photocatalyst was synthesized via electrostatic self-assembly. Its physicochemical properties were systematically investigated through morphological characterization, elemental analysis, luminescence performance, and photoelectrochemical testing. Photocatalytic degradation of 5 ppm tetracycline (TC) under long-wavelength visible light ($\lambda > 510$ nm) was achieved within 60 min, with degradation mechanisms analyzed and proposed.

(1) Structural Confirmation: XRD, TEM, HRTEM, and XPS confirmed successful preparation of CN, BOC, and their composites with high crystallinity. EDS mapping verified uniform elemental distribution in the CNBOC-2 composite, demonstrating tightly bonded interfaces and heterojunction formation.

(2) Upconversion Enhancement: PL spectra revealed strong emission at 570 nm for modified CN under 850 nm excitation, confirming superior near-infrared-to-visible light conversion. Composite samples exhibited enhanced upconversion behavior under identical conditions.

(3) Performance Metrics: The optimal CNBOC-2 composite achieved 86.2% TC degradation under $\lambda > 510$ nm within 60 min. Cycling tests confirmed excellent stability, retaining ~70% efficiency after four cycles.

ISSN 2616-5880 Vol. 6, Issue 3: 19-29, DOI: 10.25236/AJMC.2025.060302

(4) Mechanistic Insights: Nitrogen defects in CN act as intermediate states, enabling sequential low-energy photon absorption for high-energy photon emission to activate BOC. The heterojunction structure facilitates efficient electron-hole separation/migration, synergistically boosting photocatalytic activity.

References

[1] Alok A, Chaudhury N K. Tetracycline hydrochloride: A potential clinical drug for radioprotection [J]. Chemico-Biological Interactions, 2016, 245: 90-99.

[2] Yao K, Fang L, Liao P, et al. Ultrasound-activated peracetic acid to degrade tetracycline hydrochloride: Efficiency and mechanism [J]. Separation and Purification Technology, 2023, 306: 122635.

[3] Zhu W, Zhu X, Shen W, et al. Synthesis of Mn-ZIF-67 for efficient degradation of tetracycline [J]. Journal of Material Cycles and Waste Management, 2024, 26(5): 2910-2921.

[4] Li Z, Ma L, Yu M, et al. Crystalline graphitic carbon nitride in photocatalysis [J]. Surfaces and Interfaces, 2024, 51: 104492.

[5] Duan C, Xie L, Wang S, et al. Photocatalytic hydrogen evolution by degradation of organic pollutants over quantum dots doped nitrogen carbide [J]. Chemosphere, 2022, 291: 132873.

[6] Liu Y, Yu Z, Li X, et al. Super hydrophilic composite membrane with photocatalytic degradation and self-cleaning ability based on LDH and g-C_3N_4 [J]. Journal of Membrane Science, 2021, 617: 118504.

[7] Huang Z, Chen H, Zhao L, et al. Constructing g-C_3N_4 quantum dots modified g-C_3N_4/GO nanosheet aerogel for UV-Vis-NIR driven highly efficient photocatalytic H2 production [J]. International Journal of Hydrogen Energy, 2019, 44(59): 31041-31052.

[8] Chan M-H, Chen C-W, Lee I J, et al. Near-Infrared Light-Mediated Photodynamic Therapy Nanoplatform by the Electrostatic Assembly of Upconversion Nanoparticles with Graphitic Carbon Nitride Quantum Dots [J]. Inorganic Chemistry, 2016, 55(20): 10267-10277.

[9] Yang J, Xie T, Liu C, et al. Dy(III) Doped BiOCl Powder with Superior Highly Visible-Light-Driven Photocatalytic Activity for Rhodamine B Photodegradation [J/OL] 2018, 8(9): 697.

[10] Zhao X, Liu Q, Li X, et al. Excited State Absorption Upconversion Induced by Structural Defects for Photocatalysis with a Breakthrough Efficiency [J]. Angewandte Chemie, 2023, 135(10): e202219214.

[11] Ren Y, Zhu Y, Gao S, et al. Preparation of HC/BiOCl composite photocatalyst and its visible photocatalytic performance [J]. Inorganic Chemistry Communications, 2024, 163: 112329.

[12] Zheng C, Guo Y, Zhang C, et al. Nitrogen-defective protonated porous C_3N_4 nanosheets for enhanced photocatalytic hydrogen production under visible light [J]. Applied Catalysis B: Environment and Energy, 2025, 365: 124879.

[13] Yamada Y, Tanaka H, Kubo S, et al. Unveiling bonding states and roles of edges in nitrogen-doped graphene nanoribbon by X-ray photoelectron spectroscopy [J]. Carbon, 2021, 185: 342-367.

[14] Li H, Yang C, He Y, et al. Oxygen vacancies facilitated photocatalytic detoxification of three typical contaminants over graphene oxide surface embellished BiOCl photocatalysts [J]. Advanced Powder Technology, 2023, 34(3): 103971.

[15] Grigorchenko V M, Molokeev M S, Yurev I O, et al. Properties of La2F4Se, B–LaFSe phases. Phase diagram of the LaF3–La2Se3 system [J]. Journal of Solid State Chemistry, 2024, 338: 124880.

[16] Gnanasekaran L, Pachaiappan R, Kumar P S, et al. Visible light driven exotic p (CuO) - n (TiO2) heterojunction for the photodegradation of 4-chlorophenol and antibacterial activity [J]. Environmental Pollution, 2021, 287: 117304.

[17] Chen S, Huang D, Xu P, et al. Topological transformation of bismuth vanadate into bismuth oxychloride: Band-gap engineering of ultrathin nanosheets with oxygen vacancies for efficient molecular oxygen activation [J]. Chemical Engineering Journal, 2021, 420: 127573.

[18] Xu R, Zhang Q, Wang J Y, et al. Direct current triboelectric cell by sliding an n-type semiconductor on a p-type semiconductor [J]. Nano Energy, 2019, 66: 104185.

[19] Zhong D, Liu W, Tan P, et al. Insights into the synergy effect of anisotropic {001} and {230}facets of $BaTiO_3$ nanocubes sensitized with CdSe quantum dots for photocatalytic water reduction [J]. Applied Catalysis B: Environmental, 2018, 227: 1-12.

[20] Jin Z, Yang C, Li L, et al. Rational constructing 2D/3D p-n heterojunctions to modulate hydrogen evolution efficient pathways for enhances photocatalytic hydrogen production [J]. Journal of Industrial and Engineering Chemistry, 2025, 142: 449-462.

ISSN 2616-5880 Vol. 6, Issue 3: 19-29, DOI: 10.25236/AJMC.2025.060302

[21] Khezami L, Taha K K, Ghiloufi I, et al. Adsorption and photocatalytic degradation of malachite green by vanadium doped zinc oxide nanoparticles [J]. Water Science and Technology, 2015, 73(4): 881-889.

[22] Ahn I-H, Kyhm J, Lee J, et al. An alternative method for measurement of charge carrier mobility in semiconductors using photocurrent transient response [J]. Current Applied Physics, 2019, 19(4): 498-502.

[23] Chen W, Wu S-C, Xia Z-J, et al. Mesoporous g-C_3N_4 ultrathin nanosheets coupled with QDs self-decorated $SnIn_4S_8$ homojunctions towards highly efficient photocatalytic functional transformation [J]. Journal of Alloys and Compounds, 2019, 809: 151859.

[24] Wei J, Liu Z, Zhang Y, et al. Unraveling charge transfer pathways and mechanisms in CdS@$CoWO_4$ Z-scheme heterojunction photocatalysts for high-efficiency environmental remediation [J]. Separation and Purification Technology, 2023, 306: 122644.